Video Article

Scanning Electron Microscopy of Macerated Tissue to Visualize the Extracellular Matrix

Matthew K. Stephenson[1], Sean Lenihan[2,3], Roman Covarrubias[2,3], Ryan M. Huttinger[2,3], Richard J. Gumina[2,3], Douglas B. Sawyer[4], Cristi L. Galindo[2,3]

[1]Department of Pathology, Microbiology, and Immunology, Vanderbilt University Medical Center

[2]Department of Medicine, Vanderbilt University Medical Center

[3]Division of Cardiovascular Medicine, Vanderbilt University Medical Center

[4]Cardiovascular Institute, Maine Medical Center

Correspondence to: Cristi L. Galindo at cristi.l.galindo@vanderbilt.edu

URL: http://www.jove.com/video/54005
DOI: doi:10.3791/54005

Keywords: Basic Protocol, Issue 112, Scanning electron microscopy (SEM), heart, extracellular matrix, fibrosis, decellularization, cardiac fibrosis, NaOH maceration

Date Published: 6/14/2016

Citation: Stephenson, M.K., Lenihan, S., Covarrubias, R., Huttinger, R.M., Gumina, R.J., Sawyer, D.B., Galindo, C.L. Scanning Electron Microscopy of Macerated Tissue to Visualize the Extracellular Matrix. *J. Vis. Exp.* (112), e54005, doi:10.3791/54005 (2016).

Abstract

Fibrosis is a component of all forms of heart disease regardless of etiology, and while much progress has been made in the field of cardiac matrix biology, there are still major gaps related to how the matrix is formed, how physiological and pathological remodeling differ, and most importantly how matrix dynamics might be manipulated to promote healing and inhibit fibrosis. There is currently no treatment option for controlling, preventing, or reversing cardiac fibrosis. Part of the reason is likely the sheer complexity of cardiac scar formation, such as occurs after myocardial infarction to immediately replace dead or dying cardiomyocytes. The extracellular matrix itself participates in remodeling by activating resident cells and also by helping to guide infiltrating cells to the defunct lesion. The matrix is also a storage locker of sorts for matricellular proteins that are crucial to normal matrix turnover, as well as fibrotic signaling. The matrix has additionally been demonstrated to play an electromechanical role in cardiac tissue. Most techniques for assessing fibrosis are not qualitative in nature, but rather provide quantitative results that are useful for comparing two groups but that do not provide information related to the underlying matrix structure. Highlighted here is a technique for visualizing cardiac matrix ultrastructure. Scanning electron microscopy of decellularized heart tissue reveals striking differences in structure that might otherwise be missed using traditional quantitative research methods.

Video Link

The video component of this article can be found at http://www.jove.com/video/54005/

Introduction

Fibrosis disrupts the normal myocardial collagen network, which is critical for normal mechanistic functions of cardiomyocytes [1,2] as well as for inter-cellular communication, intracellular signaling, and cell survival [3]. The development of fibrosis is a major determinant of cardiac function, and fibrotic remodeling of the cardiac interstitium arising from a variety of etiologies leads to increased left ventricular stiffness and diastolic dysfunction [4]. Myocardial fibrosis may also lead to arrhythmias, and whether the progression of fibrotic remodeling is a general or local phenomenon, it is highly associated with a poor prognosis in patients with ischemic and non-ischemic cardiomyopathy [5]. Likewise, the absence of myocardial fibrosis is a strong predictor of ventricular functional recovery and long-term survival [6].

The hallmark of fibrosis is the deposition of excess collagen, which has the tensile strength of steel [7] and can adversely affect cardiomyocyte function on multiple levels. Mechanical forces resulting from an excessively collagenous matrix can lead to cardiomyocyte atrophy [8,9], passive tissue stiffness [10], tonic contraction-induced myocardial stiffness [11-13], and reduced delivery of oxygen to the remaining population of cardiomyocytes. Gap junction coupling of cardiomyocytes and myoFbs can also compromise the heart's electrical characteristics, creating a greater risk for the development of arrhythmias [14-16]. Perivascular fibrosis alters vasomotor reactivity of intramural coronary arteries and arterioles [17] and contributes to luminal narrowing that reduces the supply of oxygen and thus the survival of cardiomyocytes [17-22]. Pathogenic fibrotic and electrical remodeling, emanating from an initial site of ischemic injury or energy imbalance, inevitably progresses to heart failure.

Cardiomyocyte necrosis initiates the fibrotic response, and subsequent adverse fibrotic remodeling can occur irrespective of etiology. Finding a way to control cardiac fibrosis would be clinically beneficial for the treatment of ischemic and idiopathic cardiomyopathies, hypertensive heart disease, hypertrophic cardiomyopathy, valvular heart disease and dystrophinopathies [23-42]. Regardless of how the fibrotic disease process begins, soluble, profibrotic factors can cross the interstitial space and provoke activation of interstitial and adventitial fibroblasts at sites remote to the initial fibrotic scar, creating a cascade effect that ultimately leads to heart failure. The optimum scenario would be to exploit the fibrillogenic process using a targeted therapeutic that can be applied during the compensative hypertrophic stage of cardiomyopathy before it progresses

to systolic pump failure, diastolic heart failure, or other end-stage outcomes. The ultimate goal would be to reverse fibrosis so that dead cardiomyocytes can be replaced and heart function restored completely.

The importance of the matrix is widely understood, yet methods to study the matrix are limited mainly to quantitative measurements of major structural components, particularly collagen, and relative levels of different matrix and matricellular proteins. This protocol highlights a rarely used technique that is useful for assessing qualitative differences in the cardiac matrix. This technique has been recently used to compare and contrast fundamental differences in heart matrices from different etiologies of heart disease (in human explants), to examine hearts from post-infarcted pigs treated with the glial growth factor (GGF) isoform of neuregulin-1β, relative to untreated animals [43], and to probe for differences in the matrices of cardiac tissues from *mdx* mice (a commonly used animal model of Duchenne Muscular Dystrophy) at different ages and compared to wild-type controls. This technique was first introduced by Drs. Caulfield and Borg in 1979 [44], but few studies have since employed this powerful technique [45-47], re-introduced here with only slight modification. This methodology is a valuable research tool, because it provides qualitative information about extracellular matrix ultrastructure that might otherwise be overlooked when simply measuring matrix component content and/or level of fibrosis.

Protocol

Ethics Statement: The protocols for animal handling were approved by the Vanderbilt Institutional Animal Care and Use Committee (IACUC, protocols number M/10/117 (swine) and M/10/219 (mice) and conducted according to AAALAC-International standards. Usage of banked human cardiac tissues was approved by the Vanderbilt University Medical Center IRB (protocol number 100887).

1. Sample Collection and Storage

1. Make fresh 4% glutaraldehyde in 0.1 M phosphate buffer (PB) solution.
   CAUTION: Glutaraldehyde is toxic, wear gloves and work in a fume hood.
   1. Make a 0.2 M stock solution of PB, pH 7.4 using 21.8 g Na_2HPO_4 and 6.4 g NaH_2PO_4. *Quantum satis* (Q.s.) to 1,000 ml dH_2O.
   2. Add 400 µl of 50% glutaraldehyde to 2.5 ml of PB stock solution and 2.1 ml dH_2O.
2. Immerse a chunk (no larger than 2 cm^2) of tissue into the 4% glutaraldehyde solution. Note: Smaller pieces can also be used but should be of sufficient size (no smaller than 5 mm^2) to be easily visualized by eye in order to facilitate later steps of the protocol.
3. Incubate at room temperature for 1 hr, then store indefinitely at 4 °C.

2. Decellularization of Heart Tissue

1. Make fresh 10% aqueous NaOH solution using 10 g NaOH pellets/100 ml dH_2O.
   CAUTION: NaOH solutions are corrosive and can cause alkali-burns, wear gloves.
2. Rinse tissue in dH_2O.
3. Incubate in 10% NaOH solution at room temperature for 6 - 10 days (until tissue changes from reddish-brown to off-white or white).
4. Rinse in dH_2O until tissue becomes transparent.
5. Immerse tissue in 1% tannic acid for 4 hr at room temperature. Use 1 ml 5% stock solution per 4 ml dH_2O.
   CAUTION: Tannic acid is a strong irritant, wear gloves.
6. Rinse in dH_2O overnight.

3. Osmication and Dehydration of Heart Tissue (in Fume Hood for Safety)

1. Make a 0.2 M stock solution of sodium cacodylate buffer using 21.4 g sodium cacodylate, 10.0 g calcium chloride and 450 ml dH_2O. Mix, then add hydrochloric acid as needed to adjust pH to 7.4. *Q.s.* to 500 ml with dH_2O.
   CAUTION: Sodium cacodylate and hydrochloric acid are toxic, wear gloves and work in a fume hood.
2. Make 2% aqueous stock solution of osmium tetroxide in fume hood for safety by dissolving 1 g osmium tetroxide crystal in 50 ml dH_2O.
   CAUTION: Osmium tetroxide is a severe inhalation hazard; vapor fixation of mucus membranes or eyeballs is possible, hence handle only in the fume hood with gloves. A splash guard is recommended.
3. Rinse tissue in 0.1 M sodium cacodylate buffer (mix stock solution 1:1 with dH_2O) for 5 min on rotator (or gentle agitation).
4. Repeat previous step twice, for a total of three buffer rinses.
5. Immerse tissue in 1% osmium tetroxide in 0.1 M sodium cacodylate buffer (mix stock sodium cacodylate and stock osmium tetroxide 1:1) on rotator for 1 hr.
6. Rinse tissue in 0.1 M sodium cacodylate buffer 3 times for 5 min each on rotator.
7. Rinse tissue using increasing concentrations of ethanol (30%, 50%, 75%, 85%, 95%, and finally 100%) for 15 min each on rotator.

4. Cross Section Surface Preparation for SEM

1. Transfer tissue in 100% ethanol to a shallow Petri dish also containing 100% ethanol.
2. Hold two very sharp razor blades such that the flats of the sides are in contact with one another and the cutting edges cross to form two sides of an equilateral triangle above the specimen. To accomplish this, use the left hand to place one blade on the far right side of the sample and cut leftward. At the same time, use the right hand to place the second blade on the far left of the sample and slice rightward. Thus, the blades will be slid against each other from opposite directions to make a single smooth cut.
3. Slide the flat blade sides against each other to make a very clean cut of the specimen with minimal distortion or tearing force, preferably exposing as large a surface area as possible without damaging the specimen.

4. Repeat for each specimen to expose the cleanest possible cross section surfaces for examination in the SEM.

5. Critical Point Drying (CPD) of Heart Tissue

1. Use a spatula or tweezers to transfer tissue to the sample holder of the critical point dryer (CPD), ensuring that tissue remains in 100% ethanol at all times. Ensure that the holder is immersed in ethanol and that the transfer is achieved with the tissue exposed to air for no more than a few seconds.
2. Operate CPD per user's manual to complete 3 purge-and-fill cycles to replace ethanol with liquid carbon dioxide.
3. Operate CPD per user's manual to achieve critical point drying of the samples and return them to atmospheric pressure with controlled venting of CO_2.

6. Mounting of Heart Tissue Specimens for SEM

1. Prepare an SEM sample stub for each specimen, by adhering a carbon adhesive tab to the top surface of the aluminum stub.
2. With the aid of a stereomicroscope, carefully adhere the specimen to the adhesive tab with the cross section surface of interest facing up (away from the tab, visible), and as close as possible to parallel with the plane of the sample stub surface. Do not probe or touch the surface of interest.
3. Break a wooden applicator stick to achieve a tapered brush, ideal for paint application. Apply silver or carbon paint at the base and sides of the specimen, to improve adherence to the stub.
4. Extend a very thin line of silver or carbon paint up to an edge of the surface of interest, to provide a charge path from the surface of interest to ground.
5. Apply 2 or 3 small dabs of silver or carbon paint around the perimeter of the carbon tab, to provide a conductive path from the carbon tab surface to the metal stub and thus to ground.
6. Allow conductive paint to dry for two hrs.
7. Operate sputter coater per user's manual to apply a relatively heavy coating (target range of 30 - 40 nm) of gold-palladium alloy or gold. Pump specimen chamber to approximately 0.1 mbar; set Timer to 40 sec. Open Set valve to the 8:00 position (moderate Argon gas flow). Press Start to initiate sputter coating at 30 mA. Purple glow discharge should be visible in the specimen chamber.

7. SEM Examination of Heart Tissue Specimens

1. Perform scanning electron microscopy at relatively low accelerating voltage to minimize imaging problems associated with poor charge dissipation in the sample (charging). Suggested initial imaging condition are: 5 kV accelerating voltage, 10 mm working distance.
2. With assistance of an experienced operator, employ increased working distance to extend depth of field in imaging conditions requiring focus of fibers in multiple focal planes, or fibers extending for considerable length in the z dimension.
    1. For the microscope used here (see **Table of Materials**), in the user interface access the Navigation tab at upper right.
    2. Access the Coordinates tab from the Stage menu. To increase working distance, enter a larger value in millimeters for the Z coordinate then click on the Go To tab to move the sample stage to the entered working distance.
3. With assistance of an experienced operator, employ specimen tilt and rotation to position the surface of interest orthogonal to the electron beam. Additional tilt of 10 to 30 degrees from this position may improve observation and documentation of the matrix structure.
    1. For the microscope used here (see **Table of Materials**), in the user interface, click and hold the right mouse button, then slide left or right to focus the specimen near the periphery of the prepared surface plane of interest, noting the focused working distance.
    2. Navigate with the Manual User Interface joystick to move near the opposing edge of the surface and repeat focus. If working distance is not approximately equal to the first position, tilt specimen to achieve approximate agreement at both locations using the Coordinates tab of the Stage menu (see 7.2) and enter a tilt value in the T coordinate.
    3. Rotate specimen ninety degrees (enter value into R Coordinate field) and repeat the process until all positions are focused at approximately the same working distance.
    Note: Variable pressure SEM may be employed to improve charge dissipation if available. High vacuum is the standard operating mode for scanning electron microscopy.

Representative Results

The highlighted technique was applied to cardiac tissues from an unused human heart transplant donor (**Figure 1**), explanted tissues from transplant recipients, hearts from wild-type and dystrophic mice (**Figure 3**), and in post-myocardial infarction heart samples from a swine model of heart injury (**Figure 2**). As shown in **Figure 1**, the human cardiac matrix is an intricate weave of cross-linked proteins that display a honeycomb-like pattern when viewed in cross section. Each 'honeycomb' structure is approximately 40 µm wide, normally circumventing a single myocyte, when considering the planar view in **Figure 1**. When connected by intercalated discs, several cardiomyocytes can be envisioned as a rod running lengthwise through the 'tunnel' when the metaphor is extended to three-dimensionality. **Figure 1** also highlights the importance of the cutting procedure, with greater precision yielding more revelatory topographical data (**Figure 1**, top left) than sections that are "smashed" during the cutting process (**Figure 1**, top right).

Removal of resident cardiac cells, blood vessels, and circulatory cells prior to SEM processing uncovers additional ultra-structural details that would be less appreciable by SEM of whole heart tissue blocks. Each individual collagenous "strut", for example (**Figure 1**, bottom panels) is apparently aligned at regular intervals and perpendicular to myofibril sarcomeres. This arrangement is suitable for helping maintain heart structure by counter-acting deformations exerted during contraction and relaxation cycles, similar to the 'warp and weft' of textiles that helps to maintain fabric body and form against stretching.

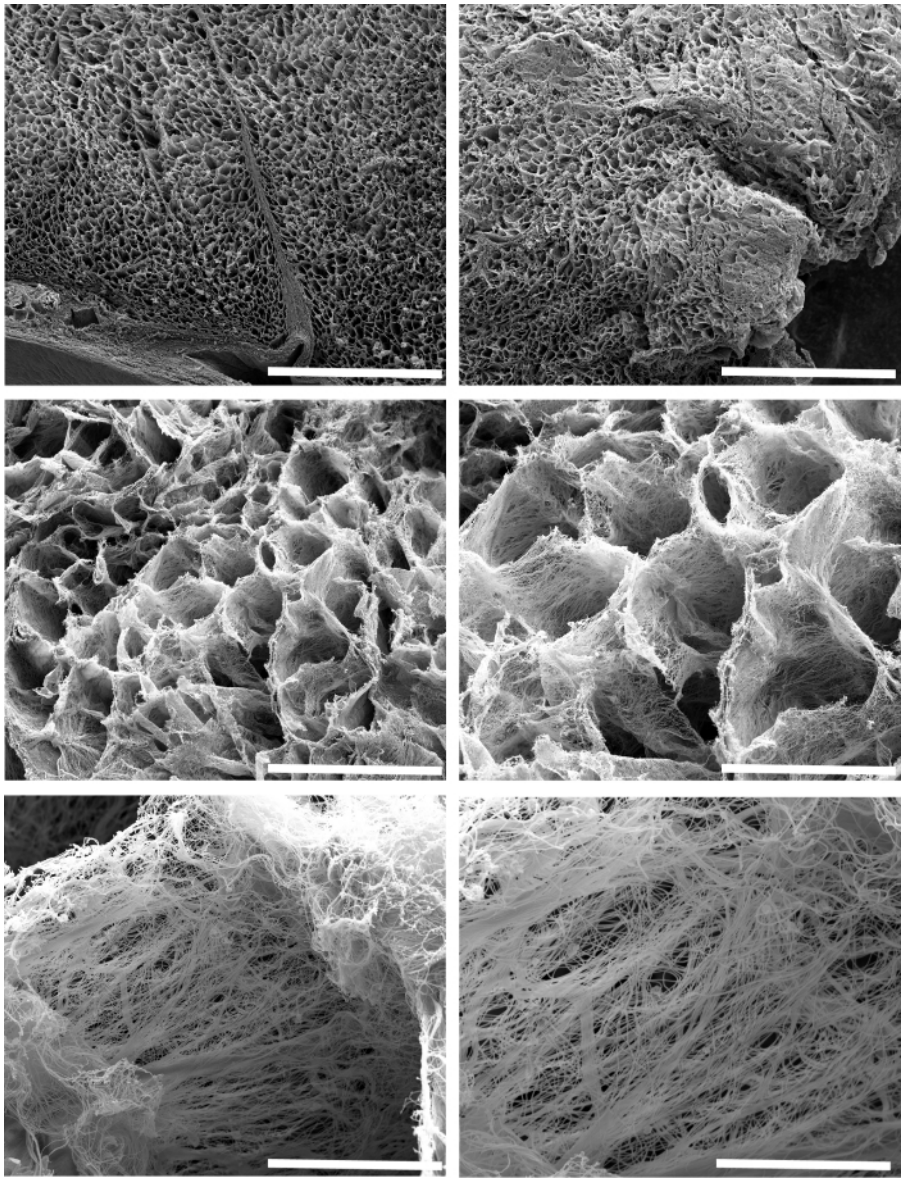

Figure 1: Representative Scanning Electron Micrographs of the Three-dimensional Arrangement of the Extracellular Matrix in Decellularized Left Ventricular Tissue Obtained from an Unused Human Donor Heart. The top two panels show the matrix in cross section at low magnification (bars = 500 µm), providing an aerial view of the architecture of normal human heart tissue. At higher magnification, one can better observe the typical honeycomb-like structure of supportive fibers that provide mechanical support for regularly spaced myofibers (middle left and right panel bars = 100 µm and 50 µm, respectively). Upon closer inspection, each 'honeycomb' is composed of fibers that are organized in parallel with one another while perpendicular to resident cardiomyocytes (bottom left and right panel bars = 10 µm and 5 µm, respectively). Please click here to view a larger version of this figure.

In addition to providing structural information, SEM of decellularized tissues can allow meaningful, qualitative assessment of extracellular matrix changes in response to injury or non-injurious forms of cardiomyopathy. For example, this technique was recently used to examine the extracellular matrices of post-infarcted swine cardiac tissues [43]. During the course of this large-animal experiment, designed specifically to assess the efficacy of the GGF2 isoform of NRG-1β as a potential therapeutic for heart failure, post-infarcted swine which received intravenous NRG-1β administration exhibited striking alterations in the cardiac matrix, compared to untreated cardiac tissues of post-infarcted animals. These results were subsequently published [43], and the technique has remained a valuable tool for building upon this initial, serendipitous discovery. **Figure 2** includes example micrographs, produced during the course of that study, which highlight drastic matrix differences between untreated and NRG-1β-treated matrices.

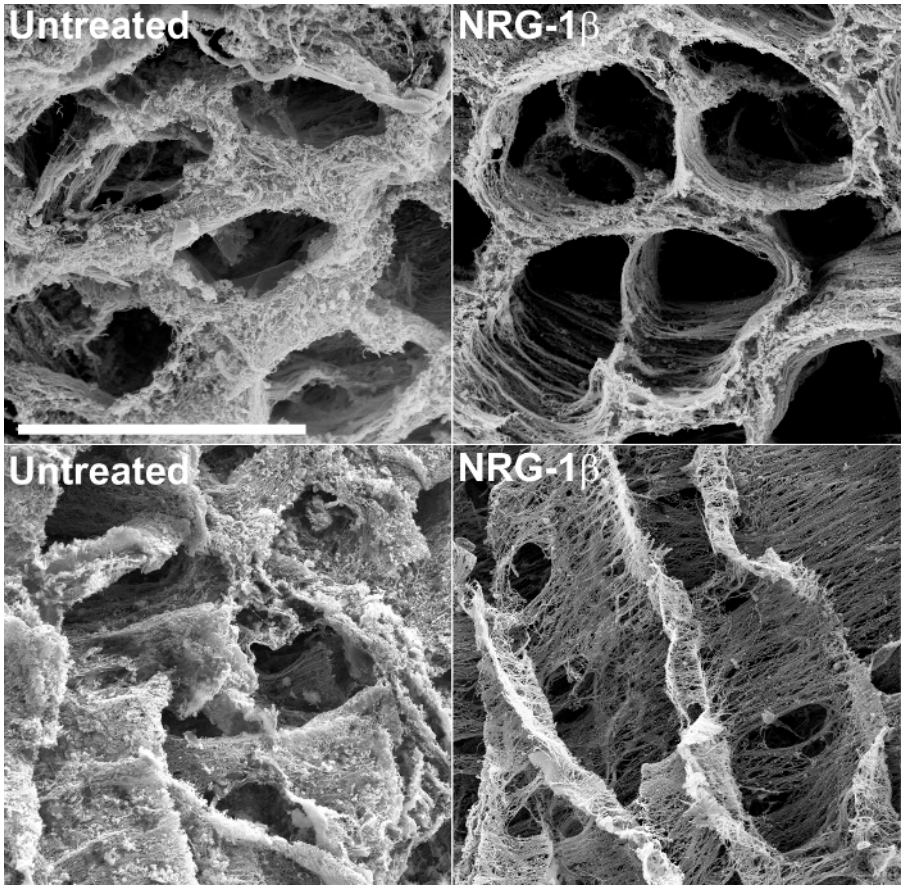

Figure 2: Representative Scanning Electron Micrographs of Left Ventricular Extracellular Matrix in Untreated and NRG-1β-treated Pigs, after NaOH Maceration. The matrix in cross section highlights the regular spatial arrangement of fibers in untreated post-myocardial infarction (post-MI) pigs (top left), compared to post-MI NRG-1β-treated animals (top right). When viewed in longitude, the matrix in untreated swine exhibits a thick, matte-like appearance (bottom left), whereas the matrix of NRG-1β-treated pigs displays regular spatial arrangement of fibers (bottom right). White bar = 40 µm (all four panels). More detailed results and figures are included in the associated manuscript [43]. Please click here to view a larger version of this figure.

Exploration of matrix changes that occur in dystrophic hearts has also yielded qualitative insights into the progression and development of an animal model of Duchenne muscular dystrophy cardiomyopathy (DMD). In *mdx* mice, a commonly used mouse model of DMD, there are significant and age-dependent differences among wild-type and *mdx* hearts when viewed by SEM after fixation and NaOH treatment. As shown in **Figure 3**, matrix components were relatively normal in 6 week-old *mdx* hearts lacking functional dystrophin relative to normal mice. More interesting, extracellular matrix organization was clearly disrupted or perhaps degraded in older dystrophin-deficient mice compared to younger *mdx* mice, illustrating the progressive nature of DMD in the heart. Such profound differences were not expected, because *mdx* mice are poorly representative of human DMD cardiomyopathy due to the fact that they exhibit a much milder cardiomyopathy phenotype and slower mortality rate than humans with DMD [48]. This suggests that even small changes in heart function can be captured using the visualization technique presented in this manuscript. This methodology should also be readily adaptable to the extracellular matrices of other organs, for which there are likewise no currently available fibrosis-targeting therapies.

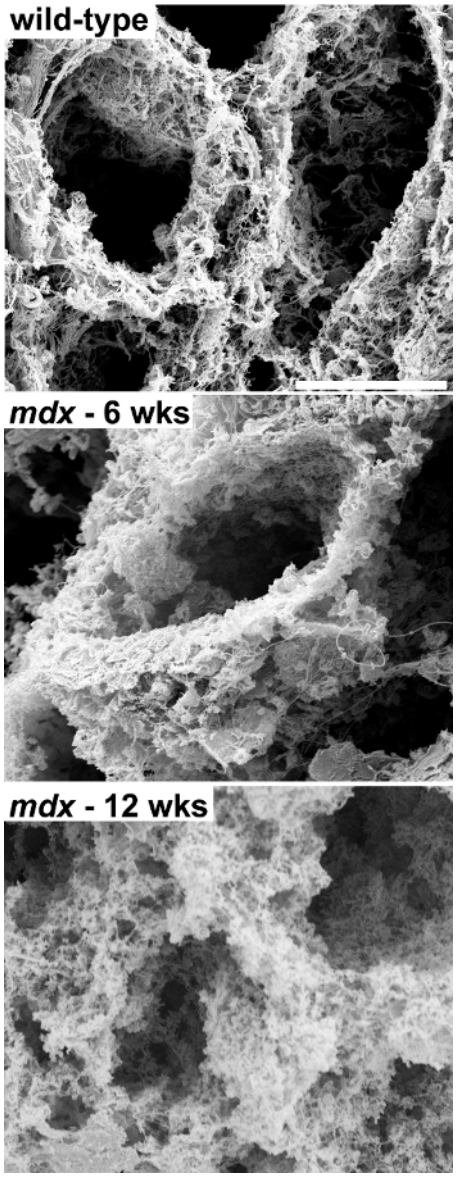

Figure 3: Representative Scanning Electron Micrographs of Left Ventricular Extracellular Matrix in Wild-type *versus mdx* Mice. The left ventricular cardiac matrix in wild-type mice (top panel) is similar to that observed in other species. The matrix in *mdx* mice at 6 weeks of age looks relatively normal, although slightly "fluffy" in appearance (middle panel). Conversely, the cardiac matrix of older *mdx* mice appears severely degenerated (bottom panel), indicating that the dystrophic process can be qualitatively captured using SEM in fixed, NaOH-macerated tissues. White bar = 10 µm (all three panels). Please click here to view a larger version of this figure.

Discussion

Cross section surface preparation is the most critical step during the protocol. To preserve fine structure, dehydrated specimens must remain in 100% ethanol at all times until introduced to the critical point drying process. Therefore the slicing of the specimens to achieve surfaces for EM examination must be done while specimens are submersed in ethanol in a shallow dish. It is also critical that the exposed surface is not touched or probed during subsequent handling. No major modifications are anticipated for application of this technique to other tissue types for similar matrix observations, although the SEM portion of the protocol might require basic electron microscopy troubleshooting regardless of sample origin. Images collected from the fibrous samples are prone to artifacts introduced by poor charge dissipation ("charging"). Charging problems can usually be minimized by reducing accelerating voltage, increasing scan speed (also called dwell time) and reducing spot size of the electron beam. Integration of several scans collected quickly enough to avoid charge artifacts will produce an image of comparable signal to noise quality without the charge artifacts present in a slower, higher quality single scan image.

This technique is inherently qualitative and thus complements when considered alongside quantitative measurements (*e.g.*, Masson's trichrome or picoserius red staining, measurement of hydroxyproline content, mass spectrometry and RNASeq) to ascertain how visualized structural differences might be related to various developmental or disease states. However, despite this limitation, the method is significant beyond cardiac fibrosis specifically, because the extracellular matrix is an essential component of almost every organ in the body. In the heart, the cardiac matrix provides critical mechanical support for continuous pumping characterized by complex stretching, twisting, and deformation,

which confers optimal entry and efflux of oxygenated and deoxygenated blood [49] for the >2.5 billion beats that occur over the average human lifespan. Given the extremely low regenerative capacity of cardiac tissue, a dynamic matrix that can be remodeled according to contextual needs makes logical sense. With only a slight stretch of the imagination, one might infer that there exist therapeutic targets for manipulating matrix remodeling to enhance the healing process, while limiting adverse fibrosis. Application of the demonstrated technique at a minimum showcases the sophistication and beauty of the cardiac matrix and in doing so further underscores its functional importance.

While the value of quantitative measures is a core principle for evaluation of practically all experimental studies, the technique highlighted here can be used to reveal qualitative ultrastructural variations that not only complement standard matrix measurements but might suggest alternate investigative paths to understand the fundamental biochemical alterations that underscore the qualitative changes. Anticipated future applications of this technique are its use in cardiac disease models and human tissues as a complementary tool for assessing matrix changes, as well as broadened usage to study other organs for which matrix changes are a component of the disease process.

Disclosures

The authors have nothing to disclose.

Acknowledgements

This study was funded by grants from the National Institutes of Health (NIH), Heart, Lung, and Blood Institute (NIHLB): K01-HL-121045, K08-HL-094703, 5T32HL007411-35, P20 HL101425, U01 HL100398.

Imaging and tissue processing (after NaOH maceration) were performed through the use of the Vanderbilt University Medical Center (VUMC) Cell Imaging Shared Resource (CISR) (supported by NIH grants CA68485, DK20593, DK58404, DK59637 and EY08126). We are especially grateful to the VUMC CISR core directors (Dr. Sam Wells and Dr. W. Gray (Jay) Jerome) for valuable technical advice and also for providing core space and resources for the purposes of filming the technique highlighted in this paper.

We would like to extend our deepest appreciation to Dr. Yan Ru Su and Ms. Kelsey Tomasek in the Cardiology Core Lab for Translational and Clinical Research at Vanderbilt University for providing technical expertise and for collecting human tissue samples used in this study.

References

1. Robinson, T. F., Cohen-Gould, L., Factor, S. M., Eghbali, M., & Blumenfeld, O. O. Structure and function of connective tissue in cardiac muscle: collagen types I and III in endomysial struts and pericellular fibers. *Scanning Microsc*. **2**, 1005-1015 (1988).
2. Robinson, T. F., Geraci, M. A., Sonnenblick, E. H., & Factor, S. M. Coiled perimysial fibers of papillary muscle in rat heart: morphology, distribution, and changes in configuration. *Circ Res*. **63**, 577-592 (1988).
3. Lunkenheimer, P. P. *et al.* The myocardium and its fibrous matrix working in concert as a spatially netted mesh: a critical review of the purported tertiary structure of the ventricular mass. *Eur J Cardiothorac Surg* **29 Suppl 1**, S41-49 (2006).
4. Wu, K. C. *et al.* Late gadolinium enhancement by cardiovascular magnetic resonance heralds an adverse prognosis in nonischemic cardiomyopathy. *J Am Coll Cardiol* **51**, 2414-2421 (2008).
5. Kramer, C. M. The expanding prognostic role of late gadolinium enhanced cardiac magnetic resonance. *J Am Coll Cardiol*. **48**, 1986-1987 (2006).
6. Park, S. *et al.* Delayed hyperenhancement magnetic resonance imaging is useful in predicting functional recovery of nonischemic left ventricular systolic dysfunction. *J Card Fail* **12**, 93-99 (2006).
7. Weber, K. T. Cardiac interstitium in health and disease: the fibrillar collagen network. *J Am Coll Cardiol*. **13**, 1637-1652 (1989).
8. Jalil, J. E., Janicki, J. S., Pick, R., Abrahams, C., & Weber, K. T. Fibrosis-induced reduction of endomyocardium in the rat after isoproterenol treatment. *Circ Res*. **65**, 258-264 (1989).
9. Fidzianska, A., Bilinska, Z. T., Walczak, E., Witkowski, A., & Chojnowska, L. Autophagy in transition from hypertrophic cardiomyopathy to heart failure. *J Electron Microsc (Tokyo)*. **59**, 181-183 (2010).
10. Lopez, B., Querejeta, R., Gonzalez, A., Larman, M., & Diez, J. Collagen cross-linking but not collagen amount associates with elevated filling pressures in hypertensive patients with stage C heart failure: potential role of lysyl oxidase. *Hypertension*. **60**, 677-683 (2012).
11. Gabbiani, G., Ryan, G. B., & Majne, G. Presence of modified fibroblasts in granulation tissue and their possible role in wound contraction. *Experientia*. **27**, 549-550 (1971).
12. Lorell, B. H. Diastolic dysfunction in pressure-overload hypertrophy and its modification by angiotensin II: current concepts. *Basic Res Cardiol*. **87 Suppl 2**, 163-172 (1992).
13. Friedrich, S. P. *et al.* Intracardiac angiotensin-converting enzyme inhibition improves diastolic function in patients with left ventricular hypertrophy due to aortic stenosis. *Circulation*. **90**, 2761-2771 (1994).
14. Rosker, C., Salvarani, N., Schmutz, S., Grand, T., & Rohr, S. Abolishing myofibroblast arrhythmogeneicity by pharmacological ablation of alpha-smooth muscle actin containing stress fibers. *Circ Res*. **109**, 1120-1131 (2011).
15. Yue, L., Xie, J., & Nattel, S. Molecular determinants of cardiac fibroblast electrical function and therapeutic implications for atrial fibrillation. *Cardiovasc Res*. **89**, 744-753 (2011).
16. Rohr, S. Myofibroblasts in diseased hearts: new players in cardiac arrhythmias? *Heart Rhythm*. **6**, 848-856 (2009).
17. Coen, M., Gabbiani, G., & Bochaton-Piallat, M. L. Myofibroblast-mediated adventitial remodeling: an underestimated player in arterial pathology. *Arterioscler Thromb Vasc Biol*. **31**, 2391-2396 (2011).
18. Brilla, C. G., Janicki, J. S., & Weber, K. T. Cardioreparative effects of lisinopril in rats with genetic hypertension and left ventricular hypertrophy. *Circulation*. **83**, 1771-1779 (1991).
19. Youn, H. J. *et al.* Relation between flow reserve capacity of penetrating intramyocardial coronary arteries and myocardial fibrosis in hypertension: study using transthoracic Doppler echocardiography. *J Am Soc Echocardiogr.***19**, 373-378 (2006).

20. Warnes, C. A., Maron, B. J., & Roberts, W. C. Massive cardiac ventricular scarring in first-degree relatives with hypertrophic cardiomyopathy. *Am J Cardiol*. **54**, 1377-1379 (1984).
21. Maron, B. J., Wolfson, J. K., Epstein, S. E., & Roberts, W. C. Intramural ('small vessel') coronary artery disease in hypertrophic cardiomyopathy. *J Am Coll Cardiol*. **8**, 545-557 (1986).
22. Olivotto, I. *et al.* Microvascular function is selectively impaired in patients with hypertrophic cardiomyopathy and sarcomere myofilament gene mutations. *J Am Coll Cardiol*. **58**, 839-848 (2011).
23. Beltrami, C. A. *et al.* Structural basis of end-stage failure in ischemic cardiomyopathy in humans. *Circulation*. **89**, 151-163 (1994).
24. Factor, S. M. *et al.* Pathologic fibrosis and matrix connective tissue in the subaortic myocardium of patients with hypertrophic cardiomyopathy. *J Am Coll Cardiol*. **17**, 1343-1351 (1991).
25. Waller, T. A., Hiser, W. L., Capehart, J. E., & Roberts, W. C. Comparison of clinical and morphologic cardiac findings in patients having cardiac transplantation for ischemic cardiomyopathy, idiopathic dilated cardiomyopathy, and dilated hypertrophic cardiomyopathy. *Am J Cardiol*. **81**, 884-894 (1998).
26. Schaper, J., Lorenz-Meyer, S., & Suzuki, K. The role of apoptosis in dilated cardiomyopathy. *Herz*. **24**, 219-224 (1999).
27. de Leeuw, N. *et al.* Histopathologic findings in explanted heart tissue from patients with end-stage idiopathic dilated cardiomyopathy. *Transpl Int*. **14**, 299-306 (2001).
28. Yoshikane, H. *et al.* Collagen in dilated cardiomyopathy--scanning electron microscopic and immunohistochemical observations. *Jpn Circ J*. **56**, 899-910 (1992).
29. Marijianowski, M. M., Teeling, P., Mann, J., & Becker, A. E. Dilated cardiomyopathy is associated with an increase in the type I/type III collagen ratio: a quantitative assessment. *J Am Coll Cardiol*. **25**, 1263-1272 (1995).
30. Pearlman, E. S., Weber, K. T., Janicki, J. S., Pietra, G. G., & Fishman, A. P. Muscle fiber orientation and connective tissue content in the hypertrophied human heart. *Lab Invest*. **46**, 158-164 (1982).
31. Huysman, J. A., Vliegen, H. W., Van der Laarse, A., & Eulderink, F. Changes in nonmyocyte tissue composition associated with pressure overload of hypertrophic human hearts. *Pathol Res Pract*. **184**, 577-581 (1989).
32. Rossi, M. A. Pathologic fibrosis and connective tissue matrix in left ventricular hypertrophy due to chronic arterial hypertension in humans. *J Hypertens*. **16**, 1031-1041 (1998).
33. Lopez, B., Gonzalez, A., Querejeta, R., Larman, M., & Diez, J. Alterations in the pattern of collagen deposition may contribute to the deterioration of systolic function in hypertensive patients with heart failure. *J Am Coll Cardiol*. **48**, 89-96 (2006).
34. Krayenbuehl, H. P. *et al.* Left ventricular myocardial structure in aortic valve disease before, intermediate, and late after aortic valve replacement. *Circulation*. **79**, 744-755 (1989).
35. Schwarz, F. *et al.* Myocardial structure and function in patients with aortic valve disease and their relation to postoperative results. *Am J Cardiol* **41**, 661-669 (1978).
36. Hein, S. *et al.* Progression from compensated hypertrophy to failure in the pressure-overloaded human heart: structural deterioration and compensatory mechanisms. *Circulation*. **107**, 984-991 (2003).
37. Brooks, W. W., Shen, S. S., Conrad, C. H., Goldstein, R. H., & Bing, O. H. Transition from compensated hypertrophy to systolic heart failure in the spontaneously hypertensive rat: Structure, function, and transcript analysis. *Genomics.* **95**, 84-92 (2010).
38. O'Hanlon, R. *et al.* Prognostic significance of myocardial fibrosis in hypertrophic cardiomyopathy. *J Am Coll Cardiol.* **56**, 867-874 (2010).
39. Green, J. J., Berger, J. S., Kramer, C. M., & Salerno, M. Prognostic value of late gadolinium enhancement in clinical outcomes for hypertrophic cardiomyopathy. *JACC Cardiovasc Imaging.* **5**, 370-377 (2012).
40. Frankel, K. A., & Rosser, R. J. The pathology of the heart in progressive muscular dystrophy: epimyocardial fibrosis. *Hum Pathol.* **7**, 375-386 (1976).
41. Otto, R. K., Ferguson, M. R., & Friedman, S. D. Cardiac MRI in muscular dystrophy: an overview and future directions. *Phys Med Rehabil Clin N Am.* **23**, 123-132, xi-xii (2012).
42. Finsterer, J., & Stollberger, C. The heart in human dystrophinopathies. *Cardiology.* **99**, 1-19 (2003).
43. Galindo, C. L. *et al.* Anti-remodeling and anti-fibrotic effects of the neuregulin-1beta glial growth factor 2 in a large animal model of heart failure. *J Am Heart Assoc.* **3**, e000773 (2014).
44. Caulfield, J. B., & Borg, T. K. The collagen network of the heart. *Lab Invest.* **40**, 364-372 (1979).
45. Ohtani, O. Three-dimensional organization of the connective tissue fibers of the human pancreas: a scanning electron microscopic study of NaOH treated-tissues. *Arch Histol Jpn.* **50**, 557-566 (1987).
46. Rossi, M. A., Abreu, M. A., & Santoro, L. B. Images in cardiovascular medicine. Connective tissue skeleton of the human heart: a demonstration by cell-maceration scanning electron microscope method. *Circulation.* **97**, 934-935 (1998).
47. Icardo, J. M., & Colvee, E. Collagenous skeleton of the human mitral papillary muscle. *Anat Rec.* **252**, 509-518 (1998).
48. McGreevy, J. W., Hakim, C. H., McIntosh, M. A., & Duan, D. Animal models of Duchenne muscular dystrophy: from basic mechanisms to gene therapy. *Dis Model Mech.* **8**, 195-213 (2015).
49. Buckberg, G., Hoffman, J. I., Mahajan, A., Saleh, S., & Coghlan, C. Cardiac mechanics revisited: the relationship of cardiac architecture to ventricular function. *Circulation.* **118**, 2571-2587 (2008).

